Materials Horizons

ROYAL SOCIETY OF CHEMISTRY

COMMUNICATION

View Article Online
View Journal | View Issue

Cite this: *Mater. Horiz.*, 2023, 10, 4232

Received 11th May 2023,
Accepted 25th July 2023

DOI: 10.1039/d3mh00718a

rsc.li/materials-horizons

3D printed microstructured ultra-sensitive pressure sensors based on microgel-reinforced double network hydrogels for biomechanical applications†

Jingxia Zheng,‡[a] Guoqi Chen,‡[a] Hailong Yang,[a] Canjie Zhu,[a] Shengnan Li,[a] Wenquan Wang,[b] Jiayuan Ren,[a] Yang Cong,[a] Xun Xu,[c] Xinwei Wang[c] and Jun Fu *[a]

Hydrogel-based wearable flexible pressure sensors have great promise in human health and motion monitoring. However, it remains a great challenge to significantly improve the toughness, sensitivity and stability of hydrogel sensors. Here, we demonstrate the fabrication of hierarchically structured hydrogel sensors by 3D printing microgel-reinforced double network (MRDN) hydrogels to achieve both very high sensitivity and mechanical toughness. Polyelectrolyte microgels are used as building blocks, which are interpenetrated with a second network, to construct super tough hydrogels. The obtained hydrogels show a tensile strength of 1.61 MPa, and a fracture toughness of 5.08 MJ m^{-3} with high water content. The MRDN hydrogel precursors exhibit reversible gel–sol transitions, and serve as ideal inks for 3D printing microstructured sensor arrays with high fidelity and precision. The microstructured hydrogel sensors show an ultra-high sensitivity of 0.925 kPa^{-1}, more than 50 times that of plain hydrogel sensors. The hydrogel sensors are assembled as an array onto a shoe-pad to monitor foot biomechanics during gaiting. Moreover, a sensor array with a well-arranged spatial distribution of sensor pixels with different microstructures and sensitivities is fabricated to track the trajectory of a crawling tortoise. Such hydrogel sensors have promising application in flexible wearable electronic devices.

New concepts

Hydrogel-based wearable flexible pressure sensors have broad application prospects in wearable devices and electronic skin. Three-dimensional (3D) printing is powerful to fabricate complicated biomimetic microstructures to improve the sensitivity and limit of detection of flexible hydrogel sensors. Recently, microgels have been widely used for 3D printing, but most 3D printed microgel constructs are weak and fragile. It is urgent and significant to improve the mechanical and sensory performances of printed sensors. In this manuscript, we demonstrate the fabrication of hierarchically structured hydrogel sensors by developing microgel-reinforced double network (MRDN) hydrogels to achieve both high sensitivity and outstanding mechanical properties. Polyelectrolyte microgels are formulated with reversible gel–sol transitions and used as inks for 3D printing of well-designed constructs. Post-printing UV curing results in super tough hydrogels interpenetrated by a second network, yielding microstructures with high fidelity and precision. The hydrogel sensors show an ultra-high sensitivity of 0.925 kPa^{-1}, more than 50 times that of plain hydrogel sensors. An array of hydrogel sensors is assembled on a shoe-pad to monitor foot biomechanics during gaiting, or track the trajectory of a crawling tortoise. It provides a promising method to utilize microgels to print high-performance microstructured sensors for wearable intelligent devices.

1. Introduction

Flexible pressure sensors with high flexibility, sensitivity and durability show great potential for continuous monitoring of human health and motion,[1,2] and have broad application prospects in wearable devices,[3,4] soft robots,[5,6] and electronic skin.[7,8] Polymer hydrogels are biomimetic biofunctional materials of a 3D cross-linked hydrophilic polymer network containing a large amount of water with adjustable physical, chemical, mechanical and electrical properties.[9–11] Therefore, polymer hydrogels have emerged as ideal materials for wearable flexible electronic devices. For application of flexible sensors in human health monitoring, such as monitoring pulse[12,13] and respiration,[14,15] and during gaiting,[16,17] it is necessary to develop hydrogels with excellent mechanical properties, sensitivity and processibility.

[a] *Key Laboratory of Polymeric Composite and Functional Materials of Ministry of Education, Guangdong Functional Biomaterials Engineering Technology Research Center, Guangzhou Key Laboratory of Flexible Electronic Materials and Wearable Devices, School of Materials Science and Engineering, Sun Yat-sen University, 135 Xingang Road West, Guangzhou 510275, China. E-mail: fujun8@mail.sysu.edu.cn*

[b] *Hospital of Stomatology, Guanghua School of Stomatology, Sun Yat-sen University, Guangzhou 510055, China*

[c] *State Key Laboratory of Polyolefins and Catalysis, Shanghai Research Institute of Chemical Industry, Shanghai 200062, China*

† Electronic supplementary information (ESI) available. See DOI: https://doi.org/10.1039/d3mh00718a

‡ J. Z. and G. C. contributed equally to this work.

One of the most important challenges for hydrogel-based flexible sensors is low sensitivity and inadequate limit of detection. Diverse microstructures have been manufactured to improve the sensitivity and limit of detection.[18] Inspired by biotissue structures of animals and plants, a variety of flexible sensors with bionic microstructures have been developed.[19,20] For example, the dermal reticular layer with spinous process surfaces is composed of two types of pressure receptors,[21] which are extremely sensitive to tiny external stimuli. This has inspired the development of a pressure sensor with a bionic spinous process microstructure.[22] The sharp structure can significantly increase the contact area under tiny pressures, achieving high sensitivity and large linear range. Besides, the complex fingerprint structure-inspired tactile sensors can accurately sense the stick-slip phenomenon during sliding and vibrating,[23] and are used to identify static, sliding states and different objects. However, microstructures based on soft and weak hydrogels are prone to damage and lose their sensory performances during cyclic loadings. There is an urgent need to develop microstructured flexible sensors with high toughness, sensitivity and stability.

Three-dimensional (3D) printing has long been a powerful technology to fabricate complicated biomimetic microstructures.[24,25] Among diverse 3D printing technologies, extrusion-based 3D bioprinting[26] is widely used to generate well-designed microstructures with high resolution and fidelity for biomimetic scaffolds and flexible sensors. Polymer hydrogels have been widely used as 3D bioprinting inks for extrusion-based printing. Usually, hydrogel precursor solutions with high viscosity are extruded from the nozzle to deposit on the substrate and immediately cured by freezing[27] or UV light.[28] In many cases, the dilemma of printability and fidelity severely limits the stability and resolution of printed constructs. Novel hydrogels are needed to achieve both printability and fidelity, as well as mechanical stability against cyclic loadings, under mild conditions.

Microgels have emerged as promising materials for 3D printing. Microgel assemblies have been used as a supporting bath to create artificial tissues and organs.[29,30] But the obtained constructs are usually weak and fragile, and need post-printing treatment to cure and improve the strength and stability. On the other hand, microgel assemblies are widely used as inks for extrusion-based 3D printing. Microgels can self-assemble through inter-particle dynamic bonds and are used as bioinks to achieve high printability, shape fidelity and cellular activity.[31] Hydrogel microparticles with extensive inter-particle hydrogen bonding and geometric jamming are developed by crushing chitosan methacrylate/polyvinyl alcohol hydrogels. The microparticles assemble into hydrogels with thixotropy and excellent creep resistance, which enables direct 3D printing at room temperature to fabricate biomimetic scaffolds with high resolution and fidelity.[27] However, the printed microgel constructs with weak inter-particle interactions cannot survive periodic loadings in practical applications. It remains a great challenge to improve the mechanical properties of the printed microgel constructs to meet the demand of hydrogel sensors on high toughness and sensing stability.

Herein, we demonstrate 3D printing of highly sensitive and tough microstructured flexible sensors based on a microgel-reinforced double network (MRDN) hydrogel for biomechanical and tracking applications. Rigid polyelectrolyte microgels have been utilized as building blocks and sacrificial units to dissipate energy, increase resistance against crack propagation and build special network topologies, and thus significantly improve the strength and toughness of hydrogels.[32,33] Here, we massively synthesize polyelectrolyte poly(2-acrylamido-2-methylpro-panesulfonic acid) (PAMPS) microgels by emulsion polymerization, and then mix them with acrylic acid (AAc) monomers to produce a viscous ink for direct 3D printing of well-designed microstructures with high resolution and fidelity. Subsequent UV curing results in *in situ* formation of a second

Jun Fu

Dr Jun Fu is a Professor at the School of Materials Science and Engineering at Sun Yat-sen University (SYSU). He obtained his BSc degree in applied chemistry at Wuhan University in 1999, and a PhD in polymer chemistry and physics from Changchun Institute of Applied Chemistry, Chinese Academy of Sciences (CAS) in 2005. He was a visiting scholar at Max Planck Institute for Polymer Research from 2005 to 2007, and a research fellow at Massachusetts General Hospital/Harvard Medical School from 2007 to 2010. He was appointed as a professor at Ningbo Institute of Materials Technology and Engineering, CAS, in 2010, and then moved to SYSU in 2019. His research focuses on high performance and functional hydrogels for biomimetic, wearable and implantable devices.

Congratulations to the 10th anniversary of Materials Horizons. It is always an inspiring platform and frontier for materials scientists. Its past ten years have been a great success. I feel very honored to receive the Materials Horizons 2020 Outstanding Paper – Runners-up Award for our paper (Materials Horizons 2020, 7, 1872–1882). I am excited to contribute this paper that uses microgels as ink to fabricate tough microstructured devices for sensors. It allows for broad extension to many other fields, including tissue engineering scaffolds, soft actuators, and flexible electronics. I sincerely wish the continued success of this esteemed journal.

network interpenetrating throughout the microgels, yielding microstructured MRDN constructs with high strength and toughness (Fig. 1). The obtained hierarchical structures improve the pressure sensitivity by a factor of 50, with outstanding stability against cyclic loadings. An array of MRDN hydrogels is assembled into a wearable shoe-pad with eight-channel pressure sensors to monitor the foot biomechanics during gaiting. Moreover, we demonstrate a dependence of sensitivity on the geometry of microstructures, including pyramids, semispheres, and cubes, and thus fabricate a flexible sensor array with well-designed in-plane distribution of different microstructures and sensitivities to track the trajectory of a moving animal (*e.g.*, a tortoise) on the surface. This study provides a promising method to fabricate microstructured hydrogel sensors with high sensitivity and stability by 3D printing of curable microgel inks. This novel strategy is promising for the development of high-performance hydrogel pressure sensors for application in wearable intelligent medical devices.

2. Results and discussion

2.1 Synthesis of microgel inks and MRDN hydrogels

Poly (2-acrylamido-2-methylpropanesulfonic acid) (PAMPS) microgels are prepared by using inverse emulsion polymerization of AMPS (Fig. 1(a)), as well as poly(acryloxyethyltrimethyl ammonium chloride) (PDAC) microgels and poly(acrylamide) (PAAm) microgels. The obtained microgels are well dispersed microspheres with an average particle diameter of about 24.2 μm and dispersity index of 8.35% (Fig. S1 and S2, ESI†). The microgels are freeze-dried into powders, which are spheres with a diameter of 1–10 μm (Fig. S3, ESI†). The dry microgels are subsequently added into an aqueous solution of acrylic acid (AAc), *N*,*N*′-methylene-bis-acrylamide (MBAA) and 2-hydroxy-4′-(2-hydroxyethoxy)-2-methylpropio-phenone (I2959) to absorb the solution overnight to achieve adequate swelling. As a result, a jammed microgel precursor solution is obtained (Fig. 1(b)), which appears as a solid-like state with shear-thinning and self-supporting properties. It can be extruded through a 210 μm diameter needle and directly printed into various constructs without a need of layer-by-layer light curing (Fig. 1(c)), which highly improves the printing efficiency. After printing, the constructs are exposed to UV light to initiate free radical polymerization of AAc monomers to form a second network interpenetrating throughout the microgels (Fig. 1(d)). On the other hand, parallel experiments are conducted to create bulk MRDN hydrogels with a PAAc network interpenetrating throughout the microgels for comparative investigations on their mechanical, conductive, and sensory performances. We observe that the polymerization time of the mic-PDAC/PAAc and mic-PAAm/PAAc hydrogels is longer than 30 minutes, while that of the mic-PAMPS/PAAc hydrogel is 15 minutes, which is advantageous for 3D printing. In addition, the mechanical properties and conductivity of mic-PAMPS/PAAc hydrogel are higher than those of the others (Fig. S5, ESI†).

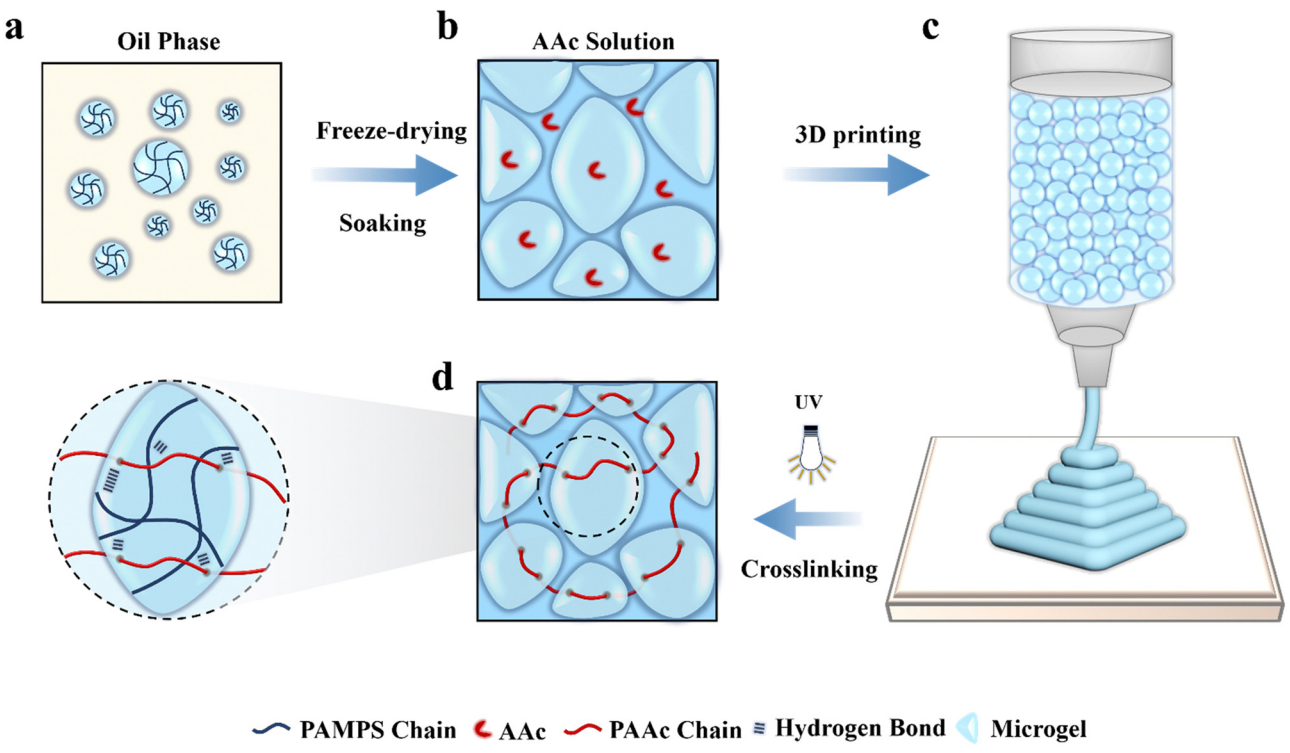

Fig. 1 PAMPS microgels for 3D printing. (a) PAMPS microgels are prepared by inverse emulsion polymerization, (b) followed by soaking in AAc solution to produce a highly swollen and jammed microgel ink (c) for extrusion-based 3D printing various microstructures; (d) post-printing curing by UV light generates a PAAc network interpenetrating throughout the PAMPS microgels, yielding microgel-reinforced double network (MRDN) hydrogel constructs with different microstructures.

Therefore, we choose PAMPS microgels with negative charges as the first network for subsequent experiments.

2.2 Rheological measurements of microgel inks

The jammed microgels exhibit high viscosity, reversible shear thinning and rapid self-healing behaviors, which are critical for direct 3D printing under ambient conditions. We carry out rheological measurements of the hydrogel precursors with different acrylic acid concentrations and 4 wt% PAMPS microgels. The rheological properties of hydrogel precursors are basically not affected by the acrylic acid concentrations (Fig. S4, ESI†). The microgel solutions below 3 wt% concentration have too low viscosity to print. We focus on microgel solutions with concentrations higher than 3 wt%. Fig. 2(a) shows that the viscosity of the jammed microgels increases with the microgel concentration and decreases as the shear rate increases from 0.01 s^{-1} to 100 s^{-1}. The jammed microgels show a shear-induced gel–fluid transition at about 10% strain (Fig. 2(b)). Dynamic strain step tests are carried out on the hydrogel with 5 wt% microgels. The microgels display a fast reversible gel–fluid transition upon cyclic shearing at 100% strain, and then the ink recovers immediately from the liquid-like state to the solid-like state at low strain (1%, Fig. 2(c)). The shear-induced reversible gel–fluid transition and rapid self-healing make the microgels ideal candidate inks for extrusion-based 3D printing.

The microgel inks can self-support after printing, which is critical for the fidelity of 3D printed hydrogel constructs, particularly for those with complex structures and large size. To evaluate this capability, creep resistance tests of hydrogel precursors are carried out (Fig. 2(d)). A continuous stress of 1 Pa (within the linear viscoelasticity region) is applied to the hydrogel precursors. The hydrogel precursor with 3 wt% microgels undergoes 5.46% deformation in 3 min and displays weak resilience in 1 min after deformation, while the precursors with 4 wt% and 5 wt% microgels exhibit much lower deformations of 0.25% and 0.12%, and that with 5 wt% microgels shows a complete recovery. These results suggest that jammed inks with higher microgel concentrations show better resistance against creep. Representative images of printed grids with different microgel concentrations visually show that a higher microgel concentration is favorable for better self-support to improve the resolution and fidelity of printed constructs (Fig. 2(e)).

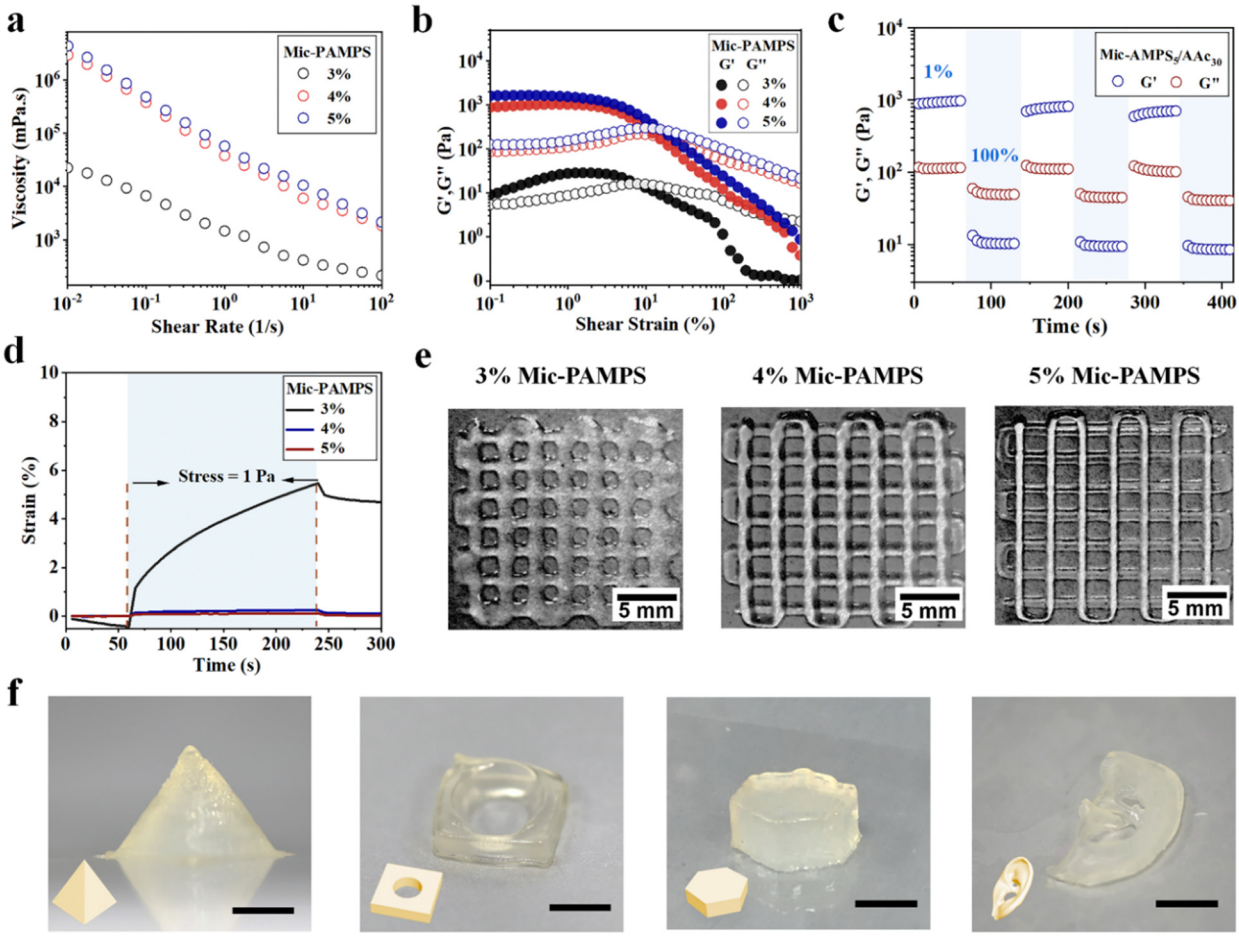

Fig. 2 Jammed microgels for 3D printing. (a) Viscosity–frequency and (b) modulus–strain scans of mic-PAMPS/PAAc solutions with different microgel concentrations. (c) Self-healing of jammed 5 wt% PAMPS microgels swollen in 30% AAc solution. (d) Representative creep and recovery curves under 1 Pa load. Representative photos of printed (e) grids of microgel inks with different concentrations, and (f) pyramid, perforated tetrahedron, hexahedron and ear. Scare bar: 5 mm.

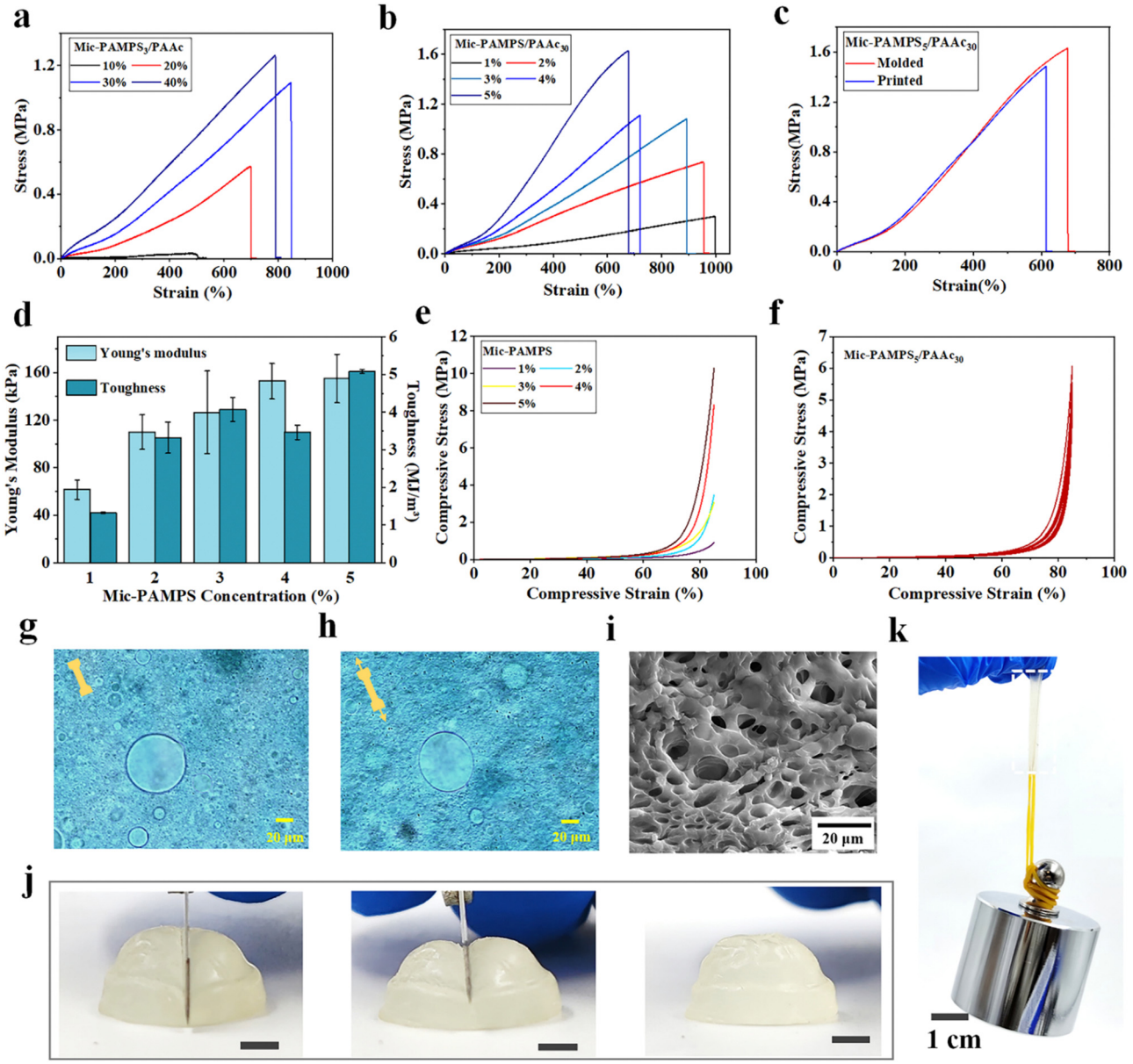

Fig. 3 Mechanical properties. Representative tensile stress–strain curves of MRDN hydrogels with varying (a) AAc and (b) microgel concentrations, and (c) prepared by injection molding or printing; (d) Young's modulus and toughness of MRDN hydrogels with 30 wt% AAc and varying microgel concentrations. (e) Representative compressive stress–strain curves of MRDN hydrogels with different microgel concentrations and (f) cyclic compressive loading–unloading curves of the Mic-PAMPS$_5$/PAAc$_{30}$ gel. Micrographs of an Alcian Blue-dyed MRDN hydrogel film at (g) 0% and (h) 100% strains. (i) SEM image of an MRDN gel. (j) Photographs showing the cutting of a printed hydrogel semisphere by using a sharp blade. Scare bar: 5 mm; (k) a printed rectangular hydrogel loaded with a 1 kg weight.

Based on the above results of rheological measurements, we choose the hydrogel precursor with 5 wt% microgels and 30 wt% AAc as the ink to print various hydrogel constructs, including pyramid, perforated tetrahedron, hexahedron, and ear with excellent fidelity and resolution (Fig. 2(f)).

2.3 Mechanical properties of MRDN hydrogels

In MRDN hydrogels, the microgels deform during stretching to dissipate energy, while the sparsely crosslinked PAAc second network interpenetrating through the microgels provides topological entanglements. To investigate the influence of hydrogel formulation on the mechanical properties, tensile and compressive tests are performed on MRDN hydrogels with different contents of microgels and AAc monomers. First, the tensile strength increases monotonically with the AAc concentrations (Fig. 3(a)). The fracture toughness is calculated by integrating the area under the stress–strain curve, and the Young's modulus is determined from the slope within the initial linear region (less than 10% strain) of the stress–strain curve. Both fracture toughness and Young's modulus increase with AAc concentration (Fig. S8, ESI†). Moreover, with the increase of PAMPS microgel content, the MRDN hydrogels show significant

enhancement in fracture strength, Young's modulus and toughness, but the fracture strain decreases due to the slightly improved rigidity of microgels (Fig. 3(b) and (d)). It is noteworthy that it presents an ultra-high tensile strength of 1.61 MPa, toughness of 5.08 MJ m^{-3}, and Young's modulus of 155 kPa for MRDN hydrogels with 5 wt% PAMPS microgels and 30 wt% AAc, where the water content is about 65%.

In order to investigate the toughening mechanism, the interactions between PAMPS microgels and AAc are investigated by using FTIR. In the corresponding FTIR spectra, the vibration absorption peaks of –NH, –C═O and –S═O show clear red shifts (Fig. S6, ESI†), which indicates hydrogen bonding between PAMPS microgels and AAc. Besides, we compare the mechanical properties of the bulk gel and the microgel-reinforced (MR) hydrogel (Fig. S7, ESI†), and find that the Young's modulus of the bulk gel is higher than that of the MR hydrogel, because PAMPS networks are highly cross-linked in microgels and may not penetrate throughout the entire double network, in sharp contrast to the bulk gel. But the fracture strain and strength of the MR hydrogel are higher than the bulk gel. We dye the anionic PAMPS microgels with cationic Alcian blue. It is observed that the microgels deform from spheres to ellipsoids along the stretching direction at 100% strain (Fig. 3(g) and (h)). SEM images of freeze-dried MRDN gels show representative porous structures with extensively linked microgels (Fig. 3(i)). The PAMPS microgel deformation and the abundant hydrogen bonds between interpenetrating networks provide an effective energy dissipation mechanism and outstanding stretchability, strength and toughness for the MRDN hydrogels.

Moreover, the MRDN hydrogels show extremely strong compression resistance. The compressive strength increases with the concentrations of PAMPS microgels (Fig. 3(e)) and AAc (Fig. S9a, ESI†), showing a compressive strength of up to 10.3 MPa at 85% strain. During cyclic loading–unloading tests, a small hysteresis loop was observed for repeated compression, showing negligible internal structure damage during compression (Fig. 3(f)). This non-hysteresis behavior is likely attributed to the deformation of microgels, which is important for the stability of mechanical and sensory performances during long-term use.

We further demonstrate that the printed constructs after post-printing curing show high strength and toughness close to those of bulk MRDN hydrogels (Fig. 3(c) and Fig. S9b, ESI†). In order to visually display the strength and toughness of printed MRDN hydrogels, we stretch a printed rectangular hydrogel sample (15 mm × 5.0 mm × 1.5 mm) to 400% strain (Fig. S10, ESI†). The rectangular hydrogel can withstand a 1 kg weight (Fig. 3(k)). More impressively, a printed hydrogel semisphere can withstand the cutting of a sharp blade and immediately restore the original state completely (Fig. 3(j)). This resistance against extreme mechanical challenge is critical for the stability of 3D printed microstructured constructs during long-term use under harsh mechanical conditions.

2.4 MRDN hydrogel sensors

The PAMPS microgel-based MRDN hydrogels are ion conductive. The conductivity decreases with the increase of the AAc content, but increases with the PAMPS microgel content (Fig. S11, ESI†). The MRDN hydrogels with 5 wt% PAMPS microgels and 30 wt% PAAc have a conductivity up to 0.84 S m^{-1}, and can act as a conductor to make the LED bulb glow (Fig. S12, ESI†).

The ion conductive MRDN hydrogels show a high strain sensitivity. The strain sensitivity, or gauge factor (GF), is defined as GF = $|\Delta R/R_0|/\varepsilon$, where ε is the strain, $\Delta R/R_0 = |R - R_0|/R_0$, with R_0 as the initial resistance and R for that under strain. When the MRDN hydrogel is stretched, the GF is 0.165 at 0–350% strain, and 0.253 at 350–460% strain (Fig. 4(a)). It responds quickly to small strain (1%) in 750–799 ms (Fig. 4(b)). In addition, based on the excellent mechanical properties of hydrogel, stable sensing signals are displayed under small strain (1–10%) and large strain (10–100%); the resistance change ratio ($\Delta R/R_0$) increases monotonically with strain (Fig. 4(c) and (d)). More importantly, the MRDN hydrogel can repeatedly and stably sense under 600 tensile cycles (Fig. 4(i)).

Similarly, the MRDN hydrogel is sensitive to external pressure. The pressure sensitivity is defined as $|\Delta R/R_0|/p$, where p is the pressure, $\Delta R/R_0 = |R - R_0|/R_0$, with R_0 as the initial resistance and R for that under strain. The pressure sensitivity of the MRDN hydrogel is 0.018 kPa^{-1} at 0–5 kPa (Fig. 4(e)). The response time to low pressure (600 Pa) is 960–1840 ms (Fig. 4(f)). Fig. 4(g) and (h) show the resistance change ratio ($\Delta R/R_0$) under different pressures. The MRDN hydrogel shows completely repeated and stable sensing signals under 600 compressive cycles (Fig. 4(j)), which is of great significance for application in flexible electronic devices.

2.5 Application in human motion monitoring

The ion conductive MRDN hydrogels with excellent sensory performances and outstanding mechanical properties enable application as wearable sensors for real-time monitoring of both subtle human activities and those with high loads like gaiting. For example, the MRDN hydrogel attached to the index finger exhibits an increase in the resistance change ratio ($\Delta R/R_0$) with finger bending angle. As the index finger restores to its original straight state, the resistance returns to the original value (Fig. 5(a)). Similarly, the hydrogel sensor can monitor the bending of wrist, elbow and knee (Fig. S13, ESI†). Moreover, the hydrogel sensor can detect subtle movements. For example, the hydrogel attached to the neck of a volunteer instantly responds to the larynx node vibration during swallowing with stable sensing signals (Fig. 5(b)).

Moreover, we attach a cylindrical hydrogel sensor to the sole in order to monitor the biomechanics during gaiting. It is interesting that the output signals show different frequencies and amplitudes during walking and running (Fig. 5(c)). These results suggest potential application of the hydrogel sensors in studies on biomechanics. For this purpose, an eight-channel pressure sensor array is assembled on a shoe-pad. The sensors are distributed on the shoe-pad in accordance to the distribution of human foot bones (Fig. 5(d)). Sensors 1 to 8 are, respectively, located under the first phalanx, the first to the fifth metatarsal, the left calcaneal and the right calcaneal bone. Fig. 5(e) shows the photographs of the assembled shoe-pad

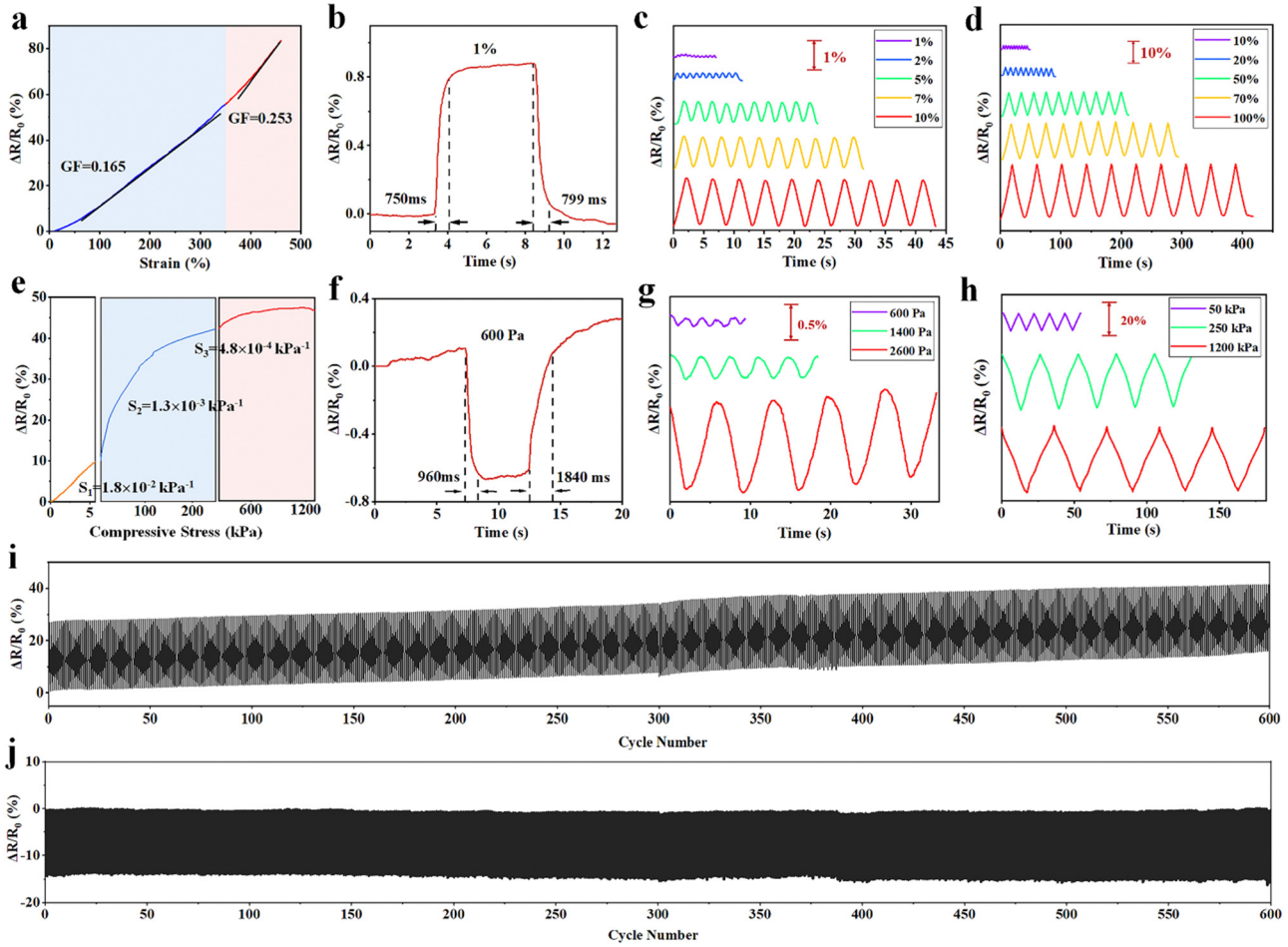

Fig. 4 Sensory performances. (a) Resistance change ratio of MRDN hydrogel during stretching. (b) The response time at 1% strain; (c) and (d) Resistance change ratios under different strains; (e) compressive pressure sensing a of MRDN hydrogel, and (f) the response time at 600 Pa; (g) and (h) Resistance change ratio at different compressive stresses. Resistance change ratio changes under 600 cyclic (i) tensile and (j) compressive tests.

(U.S size 8.5) with the pressure sensor array. A volunteer of about 70 kg wears the shoe-pad on the right foot. The sensor array provides both the static plantar pressure distribution and real-time dynamic signals through each channel during walking. When the volunteer walks, the eight channels show sequential sensing signals that clearly reflect the dynamic evolution of pressure distribution at each part of the foot (Fig. 5(f)). When the volunteer lands on the heel, the pressure is concentrated at the heel (Fig. 5(g)), and when the forefoot lands, the pressure is also distributed at the forefoot (Fig. 5(h)). The pressure distribution during successive landing during walking (Fig. 5(i)) can be quantitatively plotted into heat maps (Fig. 5(j)). The outstanding mechanical properties of the MRDN hydrogels enable the sensor array to work reliably and stably during walking. The great sensitivity of MRDN hydrogel sensors under high pressure makes it easy to distinguish different motion modes from the waveform and intensity of signals. The resolution of sensitivity distribution under the foot is limited by the pixel size of the hydrogel sensors and the capability to capture and process multi-channel signals. Such MRDN hydrogel-based sensors have numerous applications in biomechanics and intelligent medical devices.

2.6 Microstructured pressure sensors with ultra-high sensitivity

We demonstrate the fabrication of MRDN hydrogel sensors with various hierarchical microstructures by 3D printing to investigate the structure–sensitivity relationship. Different microstructure geometries such as pyramids,[34] nanowires[35] and semispheres[36] have proven to improve sensitivity and detection limits through varying contact area and stress concentrations under pressure. Here, hierarchical microstructures are fabricated by 3D printing and interpenetrating a second network throughout the microgels. The microgel precursor solution with 5 wt% PAMPS microgels and 30 wt% AAc is extrusion-printed into pyramid, hemisphere, and cube, followed by UV curing. The printed microstructured hydrogels with high resolution and fidelity have excellent mechanical properties to withstand periodic loadings, which is conducive to the stability of its structure and sensing performance.

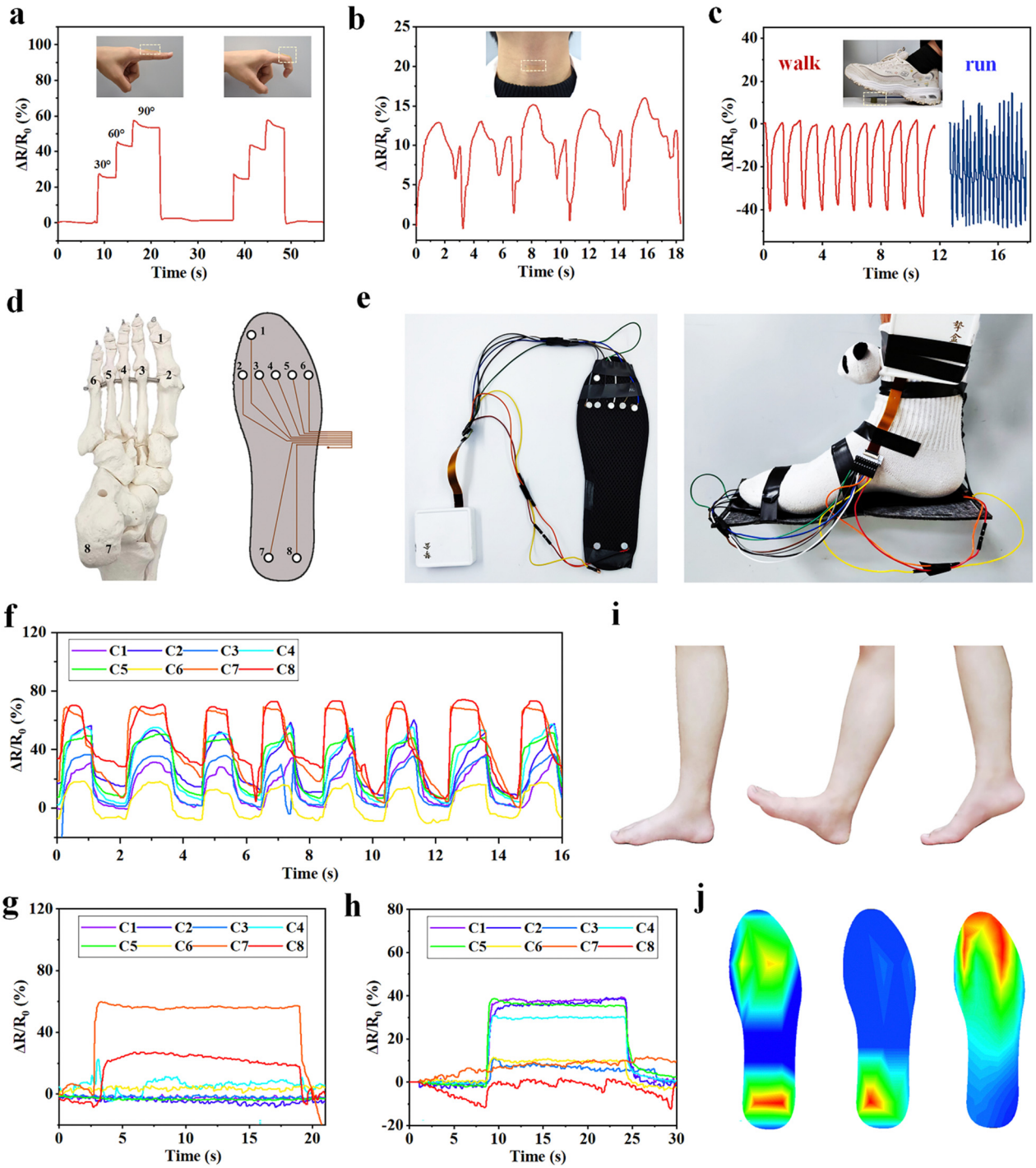

Fig. 5 Human motion monitoring. The resistance change ratio of the MRDN hydrogels attaching to human (a) finger, (b) neck and (c) sole to monitor finger bending, swallowing, walking and running. (d) Schematic diagram of human foot bones and the corresponding design of an assembled shoe-pad with eight-channel sensors. (e) Photograph of the wearable shoe-pad with eight-channel sensors for gait monitoring tests; continuous walking plantar pressure data of (f) the right foot, (g) the right heel landing; and (h) the right forefoot landing. (i) Representative photos of successive whole foot landing, heel landing, and forefoot landing, and (j) the corresponding instantaneous plantar pressure heat maps.

We test the pressure sensitivities of these microstructured sensors by loading up to 2 kPa. The pressure sensitivities of hydrogel cube, hemisphere, and pyramid on the surface (Fig. 6(b)) are 0.0274, 0.247 and 0.925 kPa^{-1} at 0–300 Pa, respectively (Fig. 6(a)). Besides, the pressure limit of detection of the pyramid microstructured hydrogel sensor is about 60 Pa, while the hemisphere microstructured sensor is about 80 Pa, and the cubic microstructured sensor is about 100 Pa (Fig. S14, ESI†). We use finite element analysis (FEA) to calculate the pressure distributions in the pyramid, hemisphere, and cube

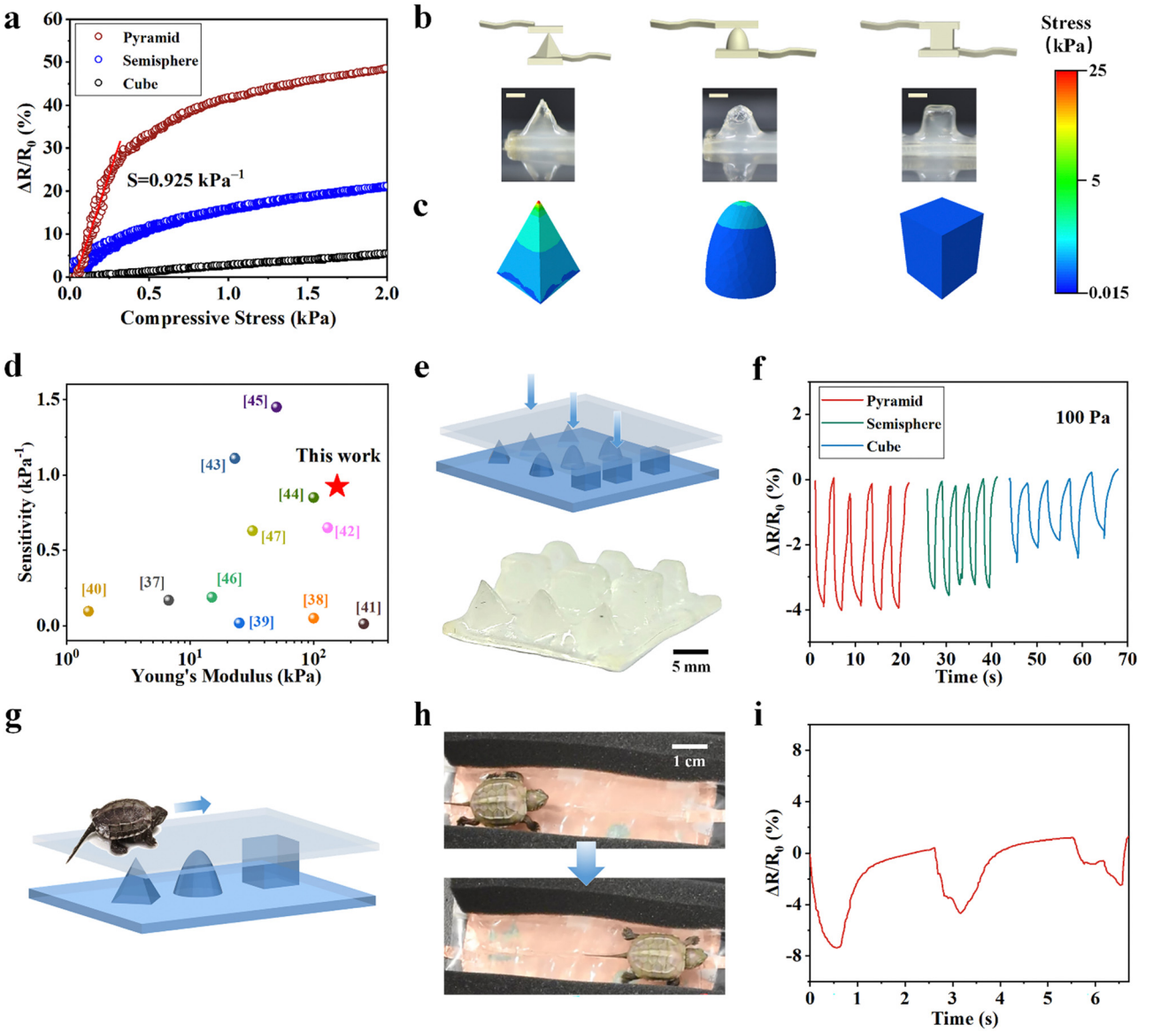

Fig. 6 Printed microstructured pressure sensor for trajectory tracking. (a) The resistance changes of (b) printed hydrogel pyramid, hemisphere, and cube. Scare bar: 5 mm, and (c) the corresponding finite element analysis (FEA) results under 1 kPa pressure. (d) Summary of sensitivity and Young's modulus of different hydrogel-based sensors. (e) Schematic and photo of a printed hydrogel array with pyramid, hemisphere, cube on the surface. (f) Resistance change ratio of the pyramid, hemisphere, and cube-like protrusions under. (g) Schematic and (h) photo of a tortoise crawling across the array of pyramid, hemisphere, and cube, and (i) the corresponding resistance change ratio along the crawling path.

pressure sensors under a pressure of 1 kPa (Fig. 6(c)). It shows a stress concentration at the top cusp area in the pyramid, whereas the stress is distributed around the dome of the hemisphere with a gradual decay downward. In contrast, the cubic shape shows a uniform pressure distribution along the height direction. These results demonstrate that sharp structures are beneficial to the high sensitivity and low limit of detection since they enable a significant increase of contact area under low-pressure loading and exhibit stress concentration. Compared with cylindrical hydrogel, the pyramid microstructure improves the pressure sensitivity by a factor of 50; such a high sensitivity is superior to most existing pressure sensors based on tough hydrogels with a high Young's modulus[37–47] (Fig. 6(d) and Table S2, ESI†), which expands its stable sensing application under low load.

Taking advantage of very high sensitivities of microstructured hydrogel sensors, we fabricated a flexible sensor array with well-designed in-plane distribution of different microstructures and sensitivities. We envision that the sensor pixels with different sensitivities will produce different signals in response to the same external force. Such a design is utilized to track the movement of living animals. We construct a proof-of-concept flexible pressure sensor array with pyramids, hemispheres and cubes on the surface by extrusion-based 3D printing with high resolution and fidelity (Fig. 6(e)). When 100 Pa load is applied to the microstructures, the pyramid structure displays a strong

sensing signal ($\Delta R/R_0 \approx 4\%$), higher than those on the hemisphere ($\Delta R/R_0 \approx 3\%$), and the cube ($\Delta R/R_0 \approx 2\%$) (Fig. 6(f)).

We further demonstrate the use of this well-designed highly sensitive sensor array to track the motions of living animals. We gently place a small tortoise (about 5 g weight) on the microstructured sensor array and track its trajectory as it crawls across the pyramids, hemispheres, and cubes (Fig. 6(g)). The real-time crawling path is recorded according to the maximum signals along its route (Fig. 6(h)). The resistance change ratio during crawling is consistent with the sensitivity of different microstructures (Fig. 6(i)). According to the different resistance change ratios rendered by crawling, we can identify the position of the small tortoise. This experiment demonstrates the feasibility to apply such a hydrogel sensor array to track motions of small living animals. Designing sensor arrays with diverse microstructures to provide sensors with higher sensitivity can greatly expand the application prospects of flexible wearable electronic devices.

3. Conclusions

In summary, a microgel-reinforced double-network (MRDN) hydrogel system for 3D printing has been developed to design highly sensitive and tough microstructured flexible sensors for human motion monitoring and tracking applications. Polyelectrolyte microgels are used as building blocks to construct super tough hydrogels through interpenetrating by a second network. The obtained hydrogels show a tensile strength of 1.61 MPa, and a fracture toughness of 5.08 MJ m^{-3} with high water content. The MRDN hydrogel precursors exhibit reversible gel–sol transitions, and serve as ideal inks for 3D printing of microstructured sensor arrays with high fidelity and precision. Thus, hierarchical structures are fabricated to improve the pressure sensitivity by a factor of 50, with outstanding structure stability against cyclic loadings. The hydrogel sensors are assembled into a wearable shoe-pad with eight-channel pressure sensors to monitor human gaiting. Moreover, we demonstrate a dependence of sensitivity on microstructures. The MRDN hydrogels are printed into a flexible sensor array with well-designed in-plane distribution of pyramids, hemispheres, and cubes. The difference in sensitivity of the microstructures is utilized to help tracking a moving animal (*e.g.*, a tortoise) on the surface. This study provides a promising method to fabricate microstructured hydrogel sensors with high sensitivity and stability by 3D printing of curable microgel inks. It is promising for the development of high-performance hydrogel pressure sensors for application in wearable devices, soft robots and electronic skin.

4. Experimental section

Experimental details and characterizations are listed in the ESI.†

Conflicts of interest

There are no conflicts to declare.

Acknowledgements

This work was supported by the National Natural Science Foundation of China (51873224), and the Ministry of Industry and Information Technology of China (TC190H3ZV/1).

Notes and references

1 Z. Liu, Y. Ma, H. Ouyang, B. Shi, N. Li, D. Jiang, F. Xie, D. Qu, Y. Zou, Y. Huang, H. Li, C. Zhao, P. Tan, M. Yu, Y. Fan, H. Zhang, Z. L. Wang and Z. Li, *Adv. Funct. Mater.*, 2019, **29**, 1807560.
2 K. Meng, X. Xiao, Z. Liu, S. Shen, T. Tat, Z. Wang, C. Lu, W. Ding, X. He, J. Yang and J. Chen, *Adv. Mater.*, 2022, **34**, 2202478.
3 M. Suneetha, O. Sun Moo, S. Mo Choi, S. Zo, K. Madhusudana Rao and S. Soo Han, *Chem. Eng. J.*, 2021, **426**, 130847.
4 Y. Ling, T. An, L. W. Yap, B. Zhu, S. Gong and W. Cheng, *Adv. Mater.*, 2020, **32**, 1904664.
5 Z. Liu, Y. Wang, Y. Ren, G. Jin, C. Zhang, W. Chen and F. Yan, *Mater. Horiz.*, 2020, **7**, 919–927.
6 M. Ilami, H. Bagheri, R. Ahmed, E. O. Skowronek and H. Marvi, *Adv. Mater.*, 2021, **33**, 2003139.
7 B. Shih, D. Shah, J. Li, T. G. Thuruthel, Y.-L. Park, F. Iida, Z. Bao, R. K. Bottiglio and M. T. Tolley, *Sci. Robot.*, 2020, **5**, 9239.
8 Y. Yu, Y. Feng, F. Liu, H. Wang, H. Yu, K. Dai, G. Zheng and W. Feng, *Small*, 2022, 2204365.
9 G. Chen, K. Wang, J. Yang, J. Huang, Z. Chen, J. Zheng, J. Wang, H. Yang, S. Li, Y. Miao, W. Wang, N. Zhu, X. Jiang, Y. Chen and J. Fu, *Adv. Mater.*, 2023, **35**, 2211716.
10 J. Y. Sun, X. Zhao, W. R. Illeperuma, O. Chaudhuri, K. H. Oh, D. J. Mooney, J. J. Vlassak and Z. Suo, *Nature*, 2012, **489**, 133–136.
11 J. Fu and M. i Panhuis, *J. Mater. Chem. B*, 2019, **7**, 1523–1525.
12 K. Meng, X. Xiao, W. Wei, G. Chen, A. Nashalian, S. Shen, X. Xiao and J. Chen, *Adv. Mater.*, 2022, **34**, 2109357.
13 X. Wang, Z. Feng, Y. Xia, G. Zhang, L. Wang, L. Chen, Y. Wu, J. Yang and Z. L. Wang, *Nano Energy*, 2022, **102**, 107710.
14 J. Wei, J. Xie, P. Zhang, Z. Zou, H. Ping, W. Wang, H. Xie, J. Z. Shen, L. Lei and Z. Fu, *ACS Appl. Mater. Interfaces*, 2021, **13**, 2952–2960.
15 J. Liu, H. Wang, T. Liu, Q. Wu, Y. Ding, R. Ou, C. Guo, Z. Liu and Q. Wang, *Adv. Funct. Mater.*, 2022, **32**, 2204686.
16 Q. Wu, Y. Qiao, R. Guo, S. Naveed, T. Hirtz, X. Li, Y. Fu, Y. Wei, G. Deng, Y. Yang, X. Wu and T. L. Ren, *ACS Nano*, 2020, **14**, 10104–10114.
17 X. Pei, H. Zhang, Y. Zhou, L. Zhou and J. Fu, *Mater. Horiz.*, 2020, **7**, 1872–1882.
18 J. Qin, L. J. Yin, Y. N. Hao, S. L. Zhong, D. L. Zhang, K. Bi, Y. X. Zhang, Y. Zhao and Z. M. Dang, *Adv. Mater.*, 2021, **33**, 2008267.
19 Y. Pang, K. Zhang, Z. Yang, S. Jiang, Z. Ju, Y. Li, X. Wang, D. Wang, M. Jian, Y. Zhang, R. Liang, H. Tian, Y. Yang and T. L. Ren, *ACS Nano*, 2018, **12**, 2346–2354.

20 S. R. A. Ruth, V. R. Feig, H. Tran and Z. Bao, *Adv. Funct. Mater.*, 2020, **30**, 2003491.
21 V. E. Abraira and D. D. Ginty, *Neuron*, 2013, **79**, 618–639.
22 S. R. A. Ruth, L. Beker, H. Tran, V. R. Feig, N. Matsuhisa and Z. Bao, *Adv. Funct. Mater.*, 2019, **30**, 1903100.
23 Y. Li, M. Zhao, Y. Yan, L. He, Y. Wang, Z. Xiong, S. Wang, Y. Bai, F. Sun, Q. Lu, Y. Wang, T. Li and T. Zhang, *npj Flexible Electron.*, 2022, **6**, 46.
24 R. L. Truby and J. A. Lewis, *Nature*, 2016, **540**, 371–378.
25 Z. Chen, D. Zhao, B. Liu, G. Nian, X. Li, J. Yin, S. Qu and W. Yang, *Adv. Funct. Mater.*, 2019, **29**, 1900971.
26 D. Chimene, R. Kaunas and A. K. Gaharwar, *Adv. Mater.*, 2020, **32**, 1902026.
27 H. Zhang, Y. Cong, A. R. Osi, Y. Zhou, F. Huang, R. P. Zaccaria, J. Chen, R. Wang and J. Fu, *Adv. Funct. Mater.*, 2020, **30**, 1910573.
28 M. Hirsch, A. Charlet and E. Amstad, *Adv. Funct. Mater.*, 2020, **31**, 2005929.
29 A. Lee, A. R. Hudson, D. J. Shiwarski, J. W. Tashman, T. J. Hinton, S. Yerneni, J. M. Bliley, P. G. Campbell and A. W. Feinberg, *Science*, 2019, **365**, 482–487.
30 O. Jeon, Y. B. Lee, H. Jeong, S. J. Lee, D. Wells and E. Alsberg, *Mater. Horiz.*, 2019, **6**, 1625–1631.
31 Q. Feng, D. Li, Q. Li, H. Li, Z. Wang, S. Zhu, Z. Lin, X. Cao and H. Dong, *ACS Appl. Mater. Interfaces*, 2022, **14**, 15653–15666.
32 Z. Y. Yuan, Z. X. Cao, C. S. Ma, R. Wu, H. T. Wu, Q. J. Xu, J. Zheng and J. R. Wu, *Chem. Eng. J.*, 2022, **450**, 138085.
33 J. Hu, T. Kurokawa, K. Hiwatashi, T. Nakajima, Z. L. Wu, S. M. Liang and J. P. Gong, *Macromolecules*, 2012, **45**, 5218–5228.
34 C. M. Boutry, A. Nguyen, Q. O. Lawal, A. Chortos, S. Rondeau-Gagne and Z. Bao, *Adv. Mater.*, 2015, **27**, 6954–6961.
35 M. K. Jonghwa Park, Y. Lee, H. S. Lee and H. Ko, *Sci. Adv.*, 2015, **1**, 1500661.
36 M. Ha, S. Lim, J. Park, D.-S. Um, Y. Lee and H. Ko, *Adv. Funct. Mater.*, 2015, **25**, 2841–2849.
37 Z. Lei, Q. Wang, S. Sun, W. Zhu and P. Wu, *Adv. Mater.*, 2017, **29**, 1700321.
38 G. Ge, Y. Zhang, J. Shao, W. Wang, W. Si, W. Huang and X. Dong, *Adv. Funct. Mater.*, 2018, **28**, 1802576.
39 S.-H. Shin, W. Lee, S.-M. Kim, M. Lee, J. M. Koo, S. Y. Hwang, D. X. Oh and J. Park, *Chem. Eng. J.*, 2019, **371**, 452–460.
40 C. Zhang, Y. Zhou, H. Han, H. Zheng, W. Xu and Z. Wang, *ACS Nano*, 2021, **15**, 1785–1794.
41 Z. Huang, X. Chen, S. J. K. O'Neill, G. Wu, D. J. Whitaker, J. Li, J. A. McCune and O. A. Scherman, *Nat. Mater.*, 2022, **21**, 103–109.
42 Z. Lei and P. Wu, *ACS Nano*, 2018, **12**, 12860–12868.
43 L. Jia, S. Wu, R. Yuan, T. Xiang and S. Zhou, *ACS Appl. Mater. Interfaces*, 2022, **14**, 27371–27382.
44 Z. Zhang, L. Tang, C. Chen, H. Yu, H. Bai, L. Wang, M. Qin, Y. Feng and W. Feng, *J. Mater. Chem. A*, 2021, **9**, 875–883.
45 X. Zhang, N. Sheng, L. Wang, Y. Tan, C. Liu, Y. Xia, Z. Nie and K. Sui, *Mater. Horiz.*, 2019, **6**, 326–333.
46 Z. Li, S. Zhang, Y. Chen, H. Ling, L. Zhao, G. Luo, X. Wang, M. C. Hartel, H. Liu, Y. Xue, R. Haghniaz, K. Lee, W. Sun, H. Kim, J. Lee, Y. Zhao, Y. Zhao, S. Emaminejad, S. Ahadian, N. Ashammakhi, M. R. Dokmeci, Z. Jiang and A. Khademhosseini, *Adv. Funct. Mater.*, 2020, **30**, 2003601.
47 S. He, B. Guo, X. Sun, M. Shi, H. Zhang, F. Yao, H. Sun and J. Li, *ACS Appl. Mater. Interfaces*, 2022, **14**, 45869–45879.

